CHEMISTRY OF MATERIALS

ARTICLE

pubs.acs.org/cm

Synthesis and Oxygen Storage Capacities of Hexagonal $Dy_{1-x}Y_xMnO_{3+\delta}$

Steven Remsen* and Bogdan Dabrowski

Department of Physics, Northern Illinois University, DeKalb, Illinois 60115, United States

ABSTRACT: Polycrystalline samples of hexagonal $P6_3cm$ (space group No. 185) $Dy_{1-x}Y_xMnO_{3+\delta}$ were synthesized over complete solubility ranges under reducing conditions with oxygen partial pressures of 5 ppm to air at high temperatures (1200−1400 °C). All samples displayed unusually large, reversible oxygen content excess ($0 \le \delta \le 0.35$) at low temperatures of ∼200−400 °C under air and oxygen atmospheres in thermogravimetric measurements. During heating, stoichiometric samples showed rapid uptakes of oxygen at 200−300 °C and equally fast releases of oxygen at 275−375 °C when materials transformed back to the stoichiometric $P6_3cm$ phase. Upon slow cooling from the stoichiometric $P6_3cm$ phase, all samples displayed rapid uptakes of oxygen at 200−350 °C. Similar changes were observed as a function of oxygen partial pressure at constant temperature. Increased, reversible changes in oxygen content were also achieved by high-pressure annealings in oxygen and hydrogen reduction at 400 °C. Thermogravimetric and X-ray diffraction measurements indicate the presence of two new structural phases at $\delta \approx 0.25$ (Hex_2) and $\delta \approx 0.40$ (Hex_3). The thermal expansion coefficient (TEC) values of the Hex_2 and $P6_3cm$ phases were determined to be $(8.4-11.6) \times 10^{-6}\,K^{-1}$ and $(2.1-5.6) \times 10^{-6}\,K^{-1}$, respectively, and the chemical expansion (CE) associated with the transition between these phases was found to be $(0.82-3.48) \times 10^{-2}$ mol^{-1}.

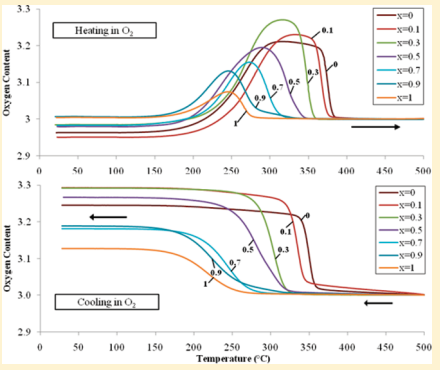

KEYWORDS: hexagonal manganites, OSC, oxygen storage/release capacities, thermal expansion, chemical expansion, nonstoichiometric oxygen content

1. INTRODUCTION

Recently, nonstoichiometric oxygen ceramic materials have been heavily researched, because of their reversible oxygen storage/release capacities (OSC) at elevated temperatures. These materials are strong candidates to compete with cryogenic distillation for commercial air separation[1] and are also being researched to improve automotive exhaust catalysts,[2] solar water splitting,[3] hydrogen−oxygen fuel cells,[4] various nonaerobic oxidation processes,[5] and assorted high-temperature production processes that require high-purity oxygen (e.g., steel, copper, plastics, glass, etc.). The development of improved oxygen storage or carrier materials is also critical to the success of new energy related technologies such as "oxy-fuel"[6] and "chemical looping"[7−9] combustion systems for "clean coal" energy production[10] and the production of synthesis gas (H_2, CO) via the partial oxidation of methane.[11]

Ideal materials for application should have large OSC values (typically measured in moles of oxygen per weight of material), and their absorption/desorption of oxygen should occur over a narrow temperature range at near-atmospheric conditions. Additional properties, such as oxygen partial pressure dependence of absorption/desorption, exothermic absorption and endothermic reduction, and stability/recoverability in reducing conditions (e.g., CO and H_2 atmospheres at high temperatures), are also desired properties. Commercially, fluorite $Ce_{1-x}Zr_xO_{2+\delta}$ compositions have been the materials of choice for air separation, which release excess oxygen ($\delta > 0$) at ∼500 °C and have OSCs of ∼400−500 μmol-O/g in oxygen atmospheres[12,13] or can be as high as 1500 μmol-O/g with 20% H_2 reversible reduction.[14] Recent studies with $Ce_{1-x}Cr_xO_{2+\delta}$ have further boosted the OSC of the fluorite structure to 2500 μmol-O/g in air and hydrogen atmospheres but require considerably higher reduction temperatures (550−700 °C) and contain toxic CrO_3.[15] Recently, hexagonal cobaltites $RBaCo_4O_{7+\delta}$ (where R = Y, Dy, Ho, Er, Tm, Yb, and Lu)[16−18] and $YBaCo_{4-x}Al_xO_{7+\delta}$[19] have been shown to have oxygen storage capacities up to ∼2700 μmol-O/g while having low reductions temperatures at ∼400−425 °C in O_2. The ease of reversible phase transitions between the hexagonal $P6_3mc$ $YBaCo_4O_7$ and orthorhombic $Pbc2_1$ $YBaCo_4O_{8.1}$ phases, which contain tetrahedrally and octahedrally coordinated cobalt,[20] is responsible for this behavior. It should also be noted that various perovskite materials ($La_{1-x}Sr_xFe_{1-x}Co_xO_{3+\delta}$ and $Ba_{0.5}Y_{0.5}MnO_{3+\delta}$, $-0.5 \le \delta \le 0$) have been demonstrated to have high OSC values (>2500 μmol-O/g) and low reoxygenation temperatures (<200 °C);[21−23] however, these materials require either high temperatures (>700 °C) or strong reducing atmospheres (e.g., H_2, CO) to form a large amount of oxygen vacancies and, therefore, their applications are more limited (e.g., chemical looping combustion or fuel reforming) than the aforementioned $Dy_{1-x}Y_xMnO_{3+\delta}$ materials, which can be used in thermal cycling under near-atmospheric conditions.

Received: March 8, 2011
Revised: July 20, 2011
Published: August 16, 2011

Rare-earth manganites and their competing hexagonal and perovskite crystal structures with 5-fold and 6-fold coordinated Mn^{3+}, respectively, have been studied for more than 50 years.[24] Conventionally, the formation of the perovskite phase versus the hexagonal phase is governed primarily by the size of the rare-earth ion in $RMnO_3$ (with constant Mn^{3+} size). During high-temperature solid-state synthesis in air, the perovskite phase forms easily with larger rare-earth elements (e.g., La, Pr, Nd, Sm, Gd, Tb, and Dy), while smaller size rare-earths (e.g., Ho, Er, Tm, Yb, Lu, and Y) favor the hexagonal phase. It has been observed that the perovskite phase is stable for a tolerance factor, $t = (R-O)/(\sqrt{2}(Mn-O))$, in the range of $0.855 \leq t \leq 1$[25] (calculated at room temperature, using Shannon's ionic size values for octahedrally coordinated Mn[26]). The perovskite structure is increasingly distorted as it approaches the lower limit of 0.855 and transforms to the hexagonal phase at $t < 0.855$.[24] $DyMnO_3$ and $YMnO_3$ have tolerance factors of 0.857 and 0.854, respectively, and will tend to form the perovskite and hexagonal phases, respectively, under normal solid-state synthesis in air, which results in substituted samples of $Dy_{1-x}Y_xMnO_3$ being on the cusp of this phase transition.

Here, we describe the synthesis of the hexagonal $P6_3cm$ phase of $Dy_{1-x}Y_xMnO_{3+\delta}$ in argon by decomposition of its competing perovskite *Pnma* phase, which was guided by our previous work on the temperature and oxygen-vacancy content dependence of the tolerance factor of perovskite manganites.[27] Hexagonal manganites have been largely believed to remain stoichiometric in oxygen content at elevated temperatures; however, our thermogravimetric measurements have demonstrated unusually large oxygen absorption at low temperature of ~200−300 °C and return to stoichiometric $P6_3cm$ phase ($\delta = 0$) above 275−375 °C in an O_2 atmosphere.[28] In addition to temperature dependence, we have observed the oxygen content of $Dy_{1-x}Y_xMnO_{3+\delta}$ to be very sensitive to changes in partial pressures of oxygen. The hexagonal phase also shows considerable stability at elevated temperatures under reducing conditions and complete recoverability from a reduced state with negative values of δ. These attributes make hexagonal $Dy_{1-x}Y_xMnO_{3+\delta}$ excellent candidates for oxygen storage applications. For comparison, our previous studies have shown that perovskite manganites with larger rare earths form small amounts of oxygen nonstoichiometry at much higher temperatures.[29] This behavior decreases for smaller rare earths, resulting in an almost-stoichiometric perovskite phase of $DyMnO_{3+\delta}$ over a wide temperature range (~20−1000 °C) in an O_2 atmosphere. Finally, the thermal and chemical expansion coefficients of hexagonal materials were measured, because these properties are relevant for application purposes.

2. EXPERIMENTAL TECHNIQUES

Synthesis was done by solid-state reaction, which is further described in the following section. Powder X-ray diffraction (XRD) measurements were made with a Rigaku D/MAX powder diffractometer in the 2θ range of 20°−70° with Cu Kα radiation. High-pressure annealings of materials after initial synthesis were done at 400 °C under 250 bar of O_2. Samples for high-pressure annealing were loaded in alumina cups inside a high-pressure containment vessel designed to be placed within a high-temperature furnace. Thermogravimetric analysis (TGA) measurements were made with Cahn TG171 and Cahn TherMax700 thermobalances in several different partial pressures of oxygen and hydrogen (balanced with argon), up to 1400 °C, at heating and cooling rates of 0.1−1.0 °C/min. TGA sample masses were ~1 g and were measured with a precision of 5 μg. Dilatometry measurements were made with a Linseis Model Differential Dilatometer L75 and samples were measured with a precision of 1 μm. Pellets with approximate dimensions of 5 mm × 3 mm × 2 mm for dilatometry measurements were cut from dense, high-temperature-sintered samples.

3. RESULTS AND DISCUSSION

3.1. Synthesis and Stability. Polycrystalline samples of hexagonal $Dy_{1-x}Y_xMnO_{3+\delta}$ were synthesized by solid-state reaction with appropriate amounts of Dy_2O_3, Y_2O_3, and MnO_2 (all with >99.99% purity). For all samples, reactants were thoroughly mixed in an agate mortar and fired in air in the temperature range of 800−1300 °C with intermediate grindings, followed by pressing the samples into high-density pellets at a pressure of ~10 kbar. All steps of the synthesis were monitored with XRD measurements and compared to previous diffraction reports in the literature of hexagonal $P6_3cm$ and perovskite *Pnma* phases of $DyMnO_3$ and $YMnO_3$.[29−32] $Dy_{1-x}Y_xMnO_{3+\delta}$ samples with x = 0.9 and 1 formed single-phase hexagonal structure in air. $Dy_{1-x}Y_xMnO_{3+\delta}$ samples that formed the perovskite or a mixed phase in air (x = 0, 0.1, 0.3, 0.5, 0.7), were then fired under ultrahigh-purity argon (99.999%) at 1300 and 1400 °C. $Dy_{1-x}Y_xMnO_{3+\delta}$ samples with x = 0 and 0.1 were then subsequently fired under ultrahigh-purity argon with a hydroxyl purifier (oxygen partial pressures of 5−10 ppm) at 1400 °C. All samples achieved the hexagonal $P6_3cm$ structure under these conditions. Figure 1 shows XRD patterns of x = 0 and 1 after synthesis of the $P6_3cm$ phase.

Considerable care was required to synthesize homogeneous Dy-rich samples. The hexagonal phase of $DyMnO_3$ has been previously achieved by epitaxially stabilized crystal growth with thin films,[33] thermal decomposition with polynuclear coordination compound precursors,[34] and quenching methods from 1600 °C in air[35] or at 1250 °C in argon for 3 days with sol−gel methods.[30] Our work confirmed that synthesis in argon at high temperature tends to favor the formation of the hexagonal phase, while synthesis in oxygen tends to favor the perovskite phase.[36] Figure 2 shows the fraction of the hexagonal phase determined from relative XRD peak intensities after several synthesis steps. Clearly, increasing reducing conditions are needed to form the hexagonal phase as the average ionic radius of the R-site cation increases. The reducing conditions needed for production of bulk polycrystalline samples of $DyMnO_3$ and $Dy_{0.1}Y_{0.9}MnO_3$ by firing methods in argon were very near to decomposition to simple oxides, and many attempts were needed to determine the most favorable temperature and length of the firings. Increased substitution of Y in $DyMnO_3$ was found to considerably ease the necessary reducing conditions to synthesize the hexagonal phase.

The oxygen content dependence of the tolerance factor, which we have previously studied for substituted $SrMnO_3$,[27] is most likely responsible for this behavior. The formation of oxygen vacancies in $RMnO_{3+\delta}$ ($\delta < 0$) causes a change in oxidation state in some of the Mn^{3+} cations to Mn^{2+}, resulting in a net $Mn^{(3+2\delta)+}$ cation, which increases the Mn−O bond length with decreasing δ. TGA measurements in oxygen were used to determine the reduced oxygen contents after synthesis of single phase hexagonal samples in argon; as will be later discussed, Figures 3 and 4, and Table 1, show the oxygen content of all samples after the final synthesis step. The resulting larger Mn−O bond lengths of these samples decrease their tolerance factor below the lower limit of 0.855 and result in the perovskite phase undergoing a phase

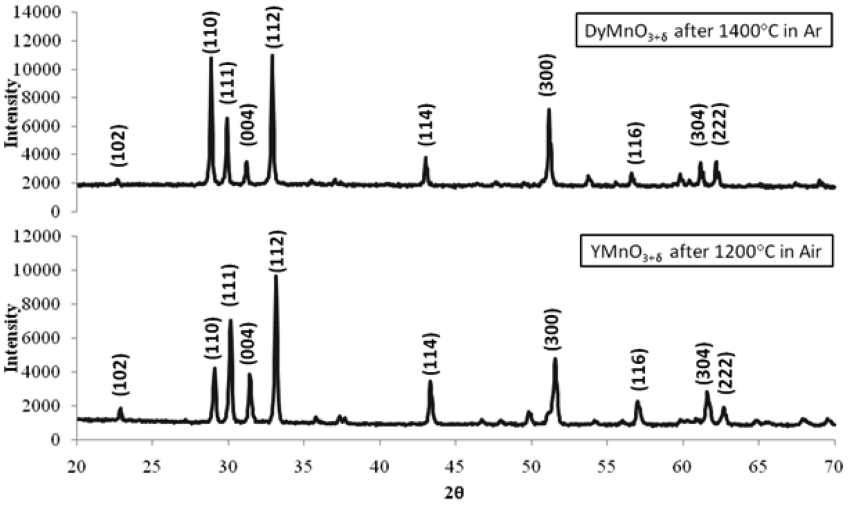

Figure 1. XRD patterns of hexagonal $DyMnO_{2.963}$ and $YMnO_{3.004}$ after synthesis.

transformation to the hexagonal phase. To have $t \leq 0.855$, using Shannon room-temperature data,[26] the minimum necessary value of δ ranges from −0.023 to −0.0027. However, we have observed that samples with such δ values did not transform completely to the hexagonal phase and slightly smaller δ values were necessary to form single-phase samples (see Table 1). Our previous in situ measurements with Ca- and La-substituted $SrMnO_3$[27,37] have shown that both Ca,Sr,La−O and Mn−O bond lengths increase with temperature in a manner that increases the value of the tolerance factor. Therefore, the transition from the perovskite phase to the hexagonal phase will most likely occur in various oxygen pressures at δ, which are a function of temperature (for example, in ∼10 ppm O_2 at 1400 °C, as we observed here, or in air at 1600 °C, as previously reported for $DyMnO_{3+\delta}$).[35] Further high-temperature in situ structural measurements should be performed to completely substantiate this dependence. Several other factors may also affect this transition. It may be enhanced by the difficultly of maintaining the 12-fold coordination of R that is required for the perovskite at high temperatures and in oxygen-deficient atmospheres, thus resulting in the 8-fold coordination of the hexagonal structure. It has also been suggested that the relative large difference in density between the perovskite and hexagonal phases may play a significant role in the relative stability of these phases.[38] The crystal strain of the perovskite phase caused by Jahn−Teller distortions may also destabilize the structure to favor the hexagonal phase, because Mn^{3+} cations are not Jahn−Teller active in the hexagonal phase's 5-fold coordinated bipyramids.

The stability of hexagonal $Dy_{1-x}Y_xMnO_{3+\delta}$ compounds was also tested by firing samples in oxygen at high temperatures of 1100−1400 °C. Since reducing conditions favor the hexagonal phase with $\delta < 0$, atmospheres that allow materials to remain near stoichiometric in oxygen content (or yield excess oxygen content, $\delta > 0$) at high temperature will favor the perovskite phase over the hexagonal phase, because of the smaller size of the $Mn^{(3+2\delta)+}$ cation. Dy-rich samples (x = 0, 0.1) began slight decomposition back to the perovskite phase at 1100 °C and completely transformed to the perovskite phase at 1400 °C. The remaining samples retained a hexagonal structure with no signs of decomposition back to the perovskite phase up to 1400 °C. These results are in agreement with the presented tolerance factor

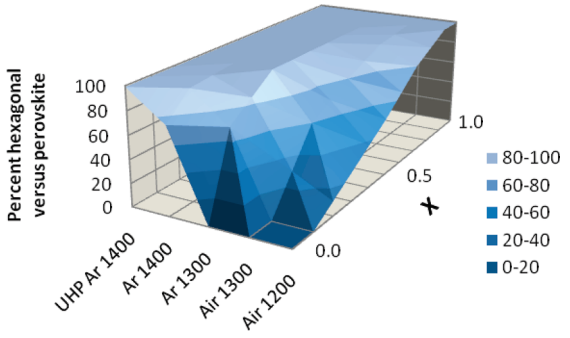

Figure 2. Phases observed during synthesis of $Dy_{1-x}Y_xMnO_{3+\delta}$.

arguments and may also explain why small rare-earth manganites (R = Y, Ho, Er, Tm, Yb, and Lu) have been observed to transform to the perovskite phase under high oxygen pressure,[39,40] while smaller A-site cations (R = Sc and In) will not transform to perovskite under similar conditions.[41]

3.2. Thermogravimetric Measurements of OSC. After initial synthesis of the hexagonal phase, all samples were annealed in TGA up to 500 °C with heating and cooling rates of 0.1−1 °C/min in various partial pressures of oxygen and hydrogen to measure OSC values and to demonstrate temperature and oxygen-partial pressure dependence of oxygen content. The oxygen content after the initial synthesis of $DyMnO_{3+\delta}$ and $YMnO_{3+\delta}$ were then determined via TGA, using the difference in weight between oxygenated samples and their respective reduction products, Dy_2O_3, Y_2O_3, and MnO (verified by XRD), obtained by first annealing in 21% O_2 at 1 °C/min and followed by slow reduction in 42% H_2/Ar at 0.1 °C/min (example of $DyMnO_{3+\delta}$ is shown in Figure 3). Thus, Figure 3 is normalized to reduction products ($\delta = -0.5$). $DyMnO_3$ and $YMnO_3$ were observed to be reduced to stable stoichiometric $P6_3cm$ phase in oxygen above 375 and 275 °C, respectively. Using this information, the oxygen content of all samples in TGA were normalized to δ = 0 above 400 °C in oxygen atmospheres. Table 2 is a compilation of OSC values achieved by the various annealing methods listed in this section.

Temperature dependence of oxygen content of $Dy_{1-x}Y_xMnO_{3+\delta}$ materials were measured in TGA with heating and cooling rates

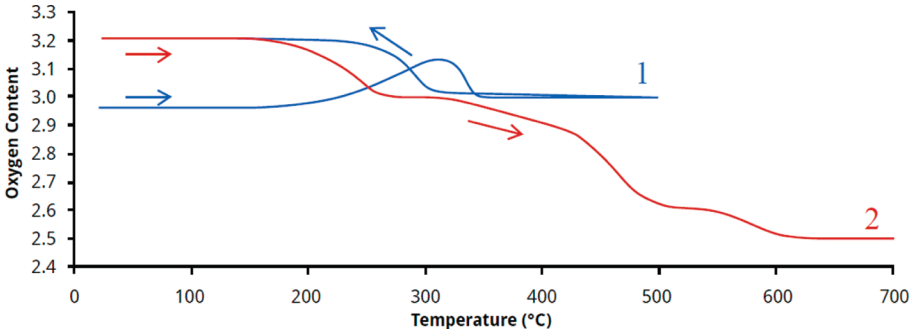

Figure 3. TGA annealing in 21% O_2 after initial synthesis in argon (curve 1) and subsequent reduction of $DyMnO_{3+\delta}$ in 42%H_2 to Dy_2O_3 and MnO (curve 2).

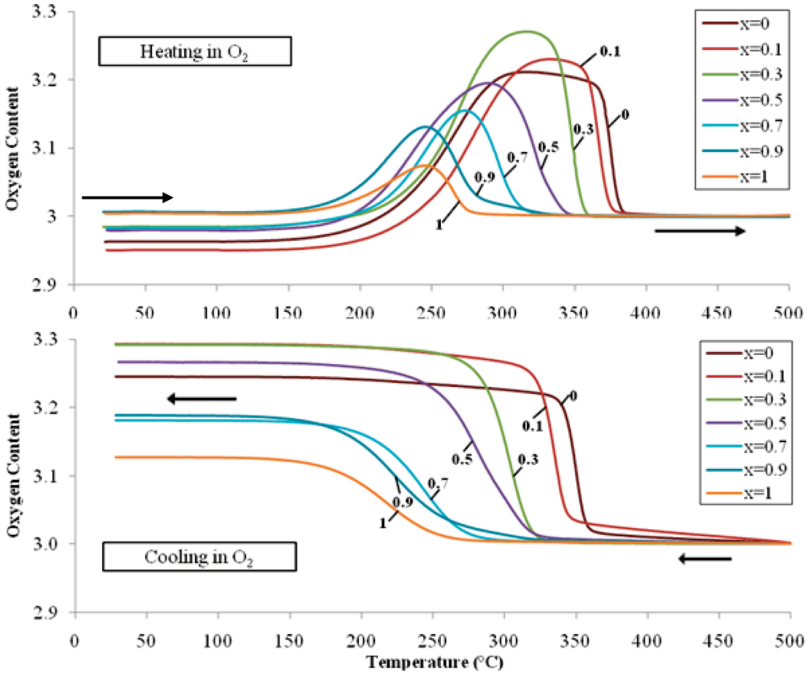

Figure 4. TGA oxygen content versus temperature for $Dy_{1-x}Y_xMnO_{3+\delta}$ with heating (top) and cooling (bottom) rates of 0.1 °C/min in O_2.

of 0.1 and 1.0 °C/min under high-purity oxygen. The resulting TG curves (0.1 °C/min; see Figure 4) clearly show the reversible absorption and desorption of oxygen below 400 °C in a narrow temperature range. OSC values were measured by the difference in oxygen content between the stoichiometric $P6_3cm$ phase observed above 400 °C (δ = 0) and the final oxygen content after cooling (δ = 0.01−0.29), which yielded a large range of values (54−1200 μmol-O/g; see Table 2). Comparing the heating and cooling rates of 0.1 °C/min versus 1.0 °C/min, the resultant TGA curves, and OSC values, indicate that oxygen absorption rates increased with Dy content. Yet, the x = 0.1, 0.3, 0.5 samples were able to achieve higher oxygen content than the pure Dy sample during cooling at a rate of 0.1 °C/min. Y-rich samples (x = 0.7, 0.9, and 1) were also able to yield larger OSC values than observed in TGA when long isothermal steps were used with slow cooling. This indicates that, if given enough time (>24 h), these samples would reach excess oxygen contents, up to $\delta \approx 0.25$. Four different temperatures were also identified from TGA curves in

Table 1. Hexagonal−Perovskite Transition δ-Values[a,b]

x	δ_{Theo}	δ_{obs}	$t(\delta_{obs})$
0	−0.0230	−0.037(0)	0.852(8)
0.1	−0.0201	−0.049(3)	0.847(0)
0.3	−0.0143	−0.015(1)	0.854(9)
0.5	−0.0085	−0.020(9)	0.853(1)
0.7	−0.0027	−0.017(1)	0.852(7)

[a] Data taken from ref 26. [b] From condition $t(\delta_{Theo}) = 0.855$, δ_{obs} are observed values from TGA, and values of t are calculated with Shannon values.

O_2, which are plotted in Figure 5 (approximate uncertainty: ±2 °C):

- the average temperature of maximum oxygen absorption upon heating and cooling,

$$\frac{d(OxCont)}{d(Temp)} = \text{local maximum}$$

dx.doi.org/10.1021/cm2006956 |Chem. Mater. 2011, 23, 3818–3827

Table 2. Oxygen Storage Capacity (OSC) of $Dy_{1-x}Y_xMnO_{3+\delta}$[a]

	Oxygen Storage Capacity, OSC (μmol-O/g)					
	Cooling Rate = 1.0 °C/min	Cooling Rate = 0.1 °C/min	Cooling Rate = 0.1 °C/min	Isotherm	Theoretical Max.	Isotherm
atmosphere	O_2	O_2	250 bar O_2	Ar−O_2	Ar−O_2/O_2	−with H_2 reduction
x = 0.0	812	926	1327	770	1884*	+455
x = 0.1	729	1138	1388		1937*	+499*
x = 0.3	444	1200	1397	1149	2055*	+596*
x = 0.5	637	1169	1625	1091	2187*	+705
x = 0.7	133	849	1542	493	2337*	+829*
x = 0.9	176	952	1694		2501*	+972*
x = 1.0	53	666	1338	95	2606*	+1051

[a] Isotherms in Ar−O_2 were obtained near the "Transition Temp." on Figure 5, and reductions in H_2 were conducted at 400 °C (asterisk (*) indicates calculated values).

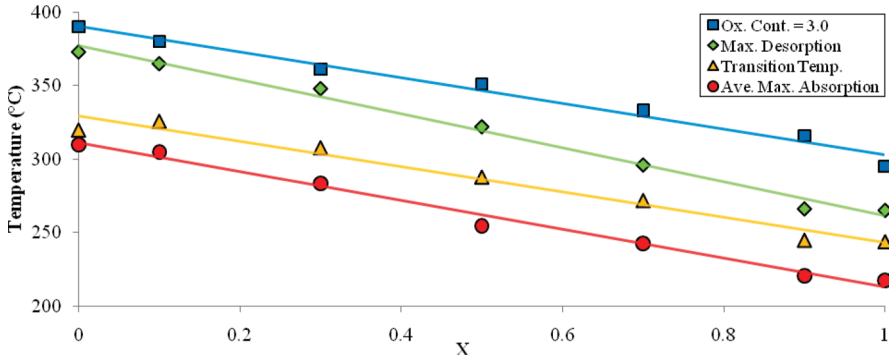

Figure 5. Temperatures relevant for oxygen storage/release for $Dy_{1-x}Y_xMnO_{3+\delta}$. See text for definitions.

- maximum oxygen desorption,

$$\frac{d(OxCont)}{d(Temp)} = \text{local minimum}$$

- transition temperature from oxygen absorption to desorption, and
- the temperature where samples return to stoichiometric composition,

$$\frac{d(OxCont)}{d(Temp)} = 0$$

(these can be approximately identified in Figure 4 by inspection). Temperature cycling over narrow temperature ranges of ~220−300 °C (x = 1) to 310−390 °C (x = 0) would produce large changes of oxygen content, i.e., large amounts of O_2 can be stored and released for various industrial processes.

Samples were also annealed at an O_2 pressure of 250 bar at 400 °C, followed by cooling to room temperatureat a rate of 0.1 °C/min. The oxygen content of these samples after annealing were determined in TGA by the difference in weight between their starting weight and their weight at 375 °C (1 °C/min heating) in 21% O_2 normalized to δ = 0 (Figure 6). All samples showed a significant increase in OSC (particularly with samples rich in Y content) achieved in high-pressure annealing versus identical cooling in 1 bar of O_2 (see Table 2). Figure 6 also reveals increased stability of oxygen content during heating in air at ~300 °C for all samples, which suggests the existence of a stable phase at $Dy_{1-x}Y_xMn^{3+}{}_{0.5}Mn^{4+}{}_{0.5}O_{3.25}$ and, possibly, the presence of another stable phase at or above an oxygen content of 3.35. XRD data of these phases for $Dy_{1-x}Y_xMnO_{3+\delta}$ (see Figure 7) indicate the formation of super structures at $\delta \approx 0.25$ (Hex_2) and $\delta \approx 0.40$ (Hex_3), which we are currently studying with neutron and synchrotron powder diffraction measurements. Although these samples show significantly increased oxygen content from atmospheric pressure oxygenations, the Mn^{3+} cation is still not completely oxidized to the Mn^{4+} state, which would be ideal for maximum OSC values. Attempts were also made to oxygenate samples (x = 0.5, 0.7, and 0.9) at higher temperature at 890 °C and 90 bar of O_2 (with a 12-h hold, followed by cooling at a rate of 10 °C/min), but these annealings yielded similar oxygen contents and the Hex_2/Hex_3 mixed phases as the high-pressure annealings at 400−500 °C. Table 2 includes these as well as theoretical values of OSC for a reversible Mn^{3+}−Mn^{4+} (δ = 0−0.5) transition. The significant increase of calculated OSC values with increased Y content seen in Table 2 is due to the smaller molar weight of Y cation and is one of the reasons why the $Dy_{1-x}Y_xMnO_{3+\delta}$ system was chosen for study after our initial work with hexagonal $DyMnO_{3+\delta}$.[42]

Oxygen partial-pressure dependence of oxygen content of $Dy_{1-x}Y_xMnO_{3+\delta}$ and absorption/desorption reversibility were demonstrated with TGA measurements during cycling in O_2 and argon atmospheres every ~12 h at various temperatures (see Figure 8). Samples were held at temperatures near their respective

dx.doi.org/10.1021/cm2006956 |Chem. Mater. 2011, 23, 3818–3827

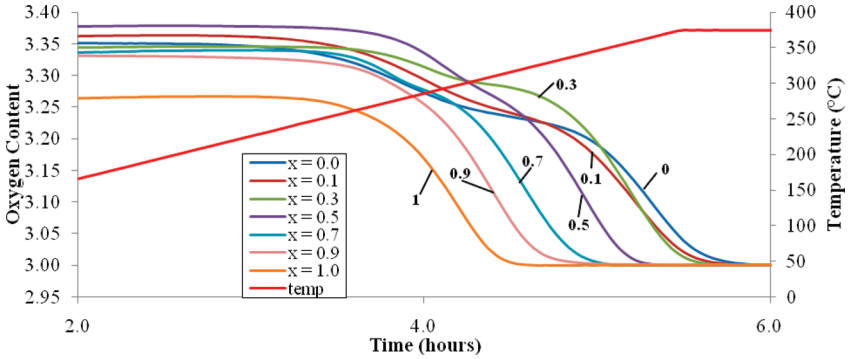

Figure 6. TGA reduction in 21% O_2 of high-pressure annealed $Dy_{1-x}Y_xMnO_{3+\delta}$ to a stable oxygen content of 3.0.

"transition temperatures" defined from Figure 5 (T = 330, 300, 280, 250, and 230 °C for x = 0, 0.3, 0.5, 0.7, and 1, respectively) and yielded OSC values of 95−1149 μmol-O/g (see Table 2). Besides $DyMnO_{3+\delta}$, which comes to equilibrium in O_2, these OSC values are comparisons of absorption after 12 h. Given more time, these samples can achieve higher oxygen content (for example, $\delta \approx 0.28$ was obtained for $Dy_{0.3}Y_{0.7}MnO_{3+\delta}$ after ~60 h). Isothermal measurements also show oxygen content to have asymptotic behavior significantly lower than achieved upon cooling (most noticeably for x = 1 and 0). Further isothermal TGA measurements at various temperatures have also shown this kinetically oxygen-content-limiting behavior, which increases equilibration time at lower temperatures (this limiting behavior accounts for the significant differences in absorption rates of Figures 4 and 7). Therefore, the OSC of the x = 0 and 1 samples would probably increase at lower temperatures and the desorption rate of x = 0.7 would most likely increase at slightly higher temperatures. The nature of these transitions from the $P6_3cm$ phase (δ = 0) to the Hex_2 phase (δ = 0.25) and from the Hex_2 phase to the Hex_3 phase (δ = 0.40) appears to easily equilibrate to intermediate oxygen content values at various oxygen partial pressures and temperatures. As a result, a mixture of several phases will occur: low temperatures (150−200 °C) may favor the Hex_3 phase; intermediate temperatures (230−330 °C) favor the Hex_2 phase; and high temperatures (above ~275−375 °C) favor the stoichiometric $P6_3cm$ phase (these ranges are dependent on the oxygen partial pressure and the Dy/Y content). The slope of oxygen content versus temperature during the $P6_3cm$−Hex_2 phase transition at constant temperature (as well as upon cooling in Figure 4) decreases with increasing Y content, which again indicates slower absorption rates of Y-rich samples. However, direct comparisons of these absorption rates are complicated by slower oxygen ion kinetics at lower temperatures, which can be approximated by $D = D_0\, e^{-E_A/(RT)}$. The lower temperatures at which the Hex_2−$P6_3cm$ phase transition occurs for Y-rich samples prevents comparisons of absorption rates at similar temperatures; thus, the differences observed in Figure 8 are due to both differences in activation energy and temperature. In addition, the increased rate of transition from the $P6_3cm$ phase to the Hex_2 phase may also be due to increased distortion to the $P6_3cm$ structure caused by larger average R-site anions. On the other hand, the transition from the Hex_2 to Hex_3 phase ($\delta \geq$ ~0.25) appears to favor Y-doped $DyMnO_{3.25}$ samples (x = 0.1, 0.3, 0.5) over pure $DyMnO_{3.25}$, as seen upon cooling in Figure 4.

Hydrogen reductions on TGA for $DyMnO_{3+\delta}$ and $YMnO_{3+\delta}$, which were initially done to determine oxygen content, showed

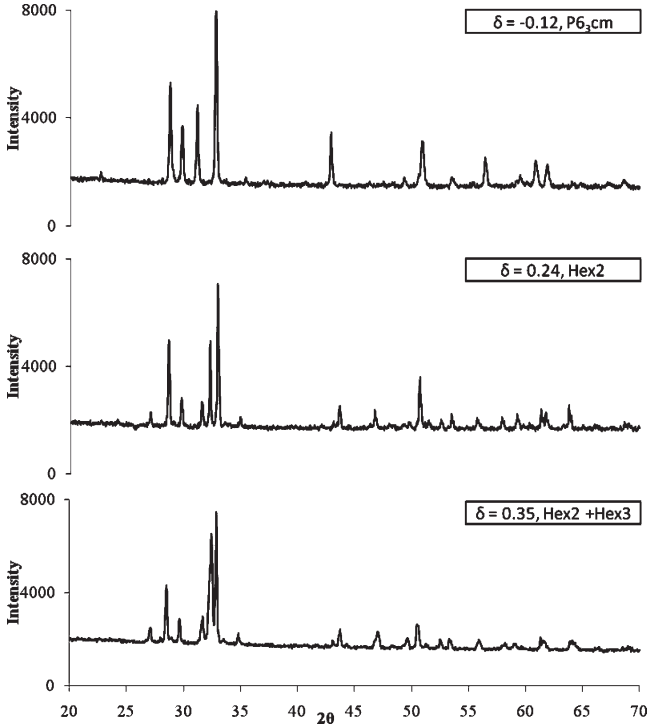

Figure 7. XRD patterns for $DyMnO_{3+\delta}$ samples: $P6_3cm$ (δ = −0.12), the Hex_2 (δ = 0.24) and mixed Hex_2 and Hex_3 phases (δ = 0.35).

the stability of both the stoichiometric phase (δ = 0) up to 300 °C and of δ = −0.12 and −0.20 on slow reduction below 420 °C, respectively (see Figure 3). Subsequently, $Dy_{0.5}Y_{0.5}MnO_{3+\delta}$ material was also reduced on TGA under identical conditions and shown to have enhanced stability at δ = 0 and δ = −0.16 on slow reduction below 420 °C. To test for recoverability of the $P6_3cm$ phase, the $DyMnO_{3+\delta}$, $Dy_{0.5}Y_{0.5}MnO_{3+\delta}$, and $YMnO_{3+\delta}$ reduced materials with these oxygen contents were prepared "in situ" at 400 °C in 42% H_2/Ar on TGA. These samples were then cooled in argon to 330, 280, and 230 °C, respectively, and then annealed at these temperatures under O_2. Samples quickly returned to stoichiometric oxygen content (>1 h) and continued to absorb oxygen, as seen during oxygen cycles in Figure 8. XRD measurements after this process confirmed that samples did not show any traces of decomposition to simple oxides. In addition, a sample of $DyMnO_{3+\delta}$ was slowly reduced on TGA in 42% H_2 at 350 °C and then fast-cooled to room

dx.doi.org/10.1021/cm2006956 |Chem. Mater. 2011, 23, 3818–3827

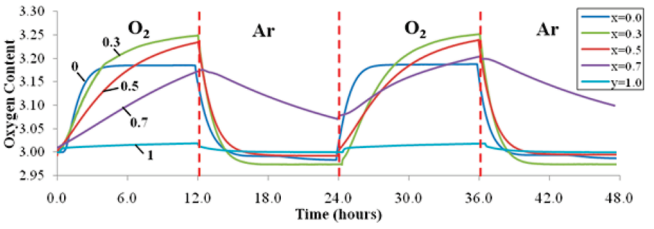

Figure 8. TGA of $Dy_{1-x}Y_xMnO_{3+\delta}$ during switching between Ar and O_2 at temperatures of 330, 300, 280, 250, and 230 °C for x = 0, 0.3, 0.5, 0.7, and 1, respectively.

temperature to synthesize a sample for XRD with an oxygen content of $\delta = -0.12$. The XRD pattern of this oxygen-deficient sample also did not show any signs of decomposition, which confirms preservation of the $P6_3cm$ phase at $\delta = -0.12$ (see Figure 7). Thus, the addition of hydrogen cycling at 400 °C to either thermal or oxygen partial-pressure cycling would yield an additional OSC of ~450−1050 μmol-O/g (for x = 0−1) and would place these materials to near-record levels of OSC, ranging from 1150 μmol-O/g to 2650 μmol-O/g (seen in Table 2; the calculated values assume the stabilities seen at $\delta = -0.12, -0.16$, and −0.20 change proportionally with x for intermediate samples).

While the values measured here do not surpass the best observed OSC in the literature and the slow oxygen kinetics of Y-rich samples (x = 0.7, 0.9, 1) may be a limiting factor for their potential use for OSC application, the $Dy_{1-x}Y_xMnO_{3+\delta}$ system does have several key advantages for application over these other candidates. First and foremost, the $Dy_{1-x}Y_xMnO_{3+\delta}$ system has the lowest reported reduction temperature, being ~25−125 °C lower than the best reported reduction temperature of $YBaCo_{4-x}Al_xO_{7+\delta}$ (with significant OSC values). Upon further comparison to $YBaCo_{4-x}Al_xO_{7+\delta}$, which decomposes at 550−700 °C in air, $Dy_{1-x}Y_xMnO_{3+\delta}$ has far superior stability, remaining stable up to 1100−1400 °C. In addition, from a hazardous waste and cost standpoint, manganese oxides is much preferable to that of cobalt or chromium oxides. Finally, large changes in Mn oxidation state in hexagonal $Dy_{1-x}Y_xMnO_{3+\delta}$ (as seen also with $YBaCo_{4-x}Al_xO_{7+\delta}$) rely on reversible phase transitions between several structures containing transition-metal ions in variable coordination, unlike the majority of OSC materials, which depend on the creation of oxygen-ion vacancies or interstitial sites at high temperatures. The potential OSC of related hexagonal manganites could easily surpass the current highest reported values, if they can be modified by chemical substitution to easily and reversibly transition between phases with large amounts of Mn^{2+} and Mn^{4+} at low temperatures.

Finally, apart from any possible OSC application, it should be noted that hexagonal manganites have been largely believed, to the best of our knowledge, to remain stoichiometric in oxygen content at elevated temperatures. In situ structural measurements at high temperatures have reported a displacement of the MnO_5 bipyramids and a transition to the $P6_3/mmc$ structure, which occur for $YMnO_3$ at ~650 °C and ~950 °C, respectively.[43,44] Slight excesses of oxygen content ($\delta \approx 0.01$) have been reported at 1200 °C for $YMnO_{3+\delta}$ and $ErMnO_{3+\delta}$[45] but not at the lower temperatures, as we have observed with thermogravimetric and XRD measurements. This behavior may not have been previously observed in other hexagonal manganites due to the narrow range of temperatures (~200−350 °C) at which these new phases exist upon heating before returning back to $\delta = 0$ above ~350 °C and the slow cooling or high oxygen partial pressures that they require. This temperature range has not been of particular interest for structural and multiferroic studies of $RMnO_3$, as most studies have been done either at low temperature, to study magnetic ordering (≤200 K), or at high temperature, to measure the rattling behavior of the MnO_5 bipyramids or structural transitions (≥500 °C).[46−54] Our results indicate that the hexagonal $RMnO_{3+\delta}$ family is most likely prone to considerable oxygen nonstoichiometry and also suggest a direct relationship between reduction temperature and sorption rates of oxygen to the average ionic size of R. If this is the case, other hexagonal $RMnO_{3+\delta}$ materials with rare earths that are close in ionic size to that of Y (e.g., Ho and Er) will have similar nonstoichiometric behavior. It should be noted that our synthesis of $YMnO_{3+\delta}$ under fast cooling to room temperature yielded small, but measurable, excesses in oxygen content (δ = 0.004). Many studies of $RMnO_{3+\delta}$ use samples prepared at elevated temperature, followed by various cooling rates, which would yield slightly nonstoichiometric samples for low-temperature measurements. Properties associated with excess oxygen content (e.g., disruptions to the exchange interaction or the presence of Mn^{4+}) may very well have had a significant impact on the multiferroic properties of these samples, because we have observed that even slight oxygen and cation nonstoichiometries can have profound effects on magnetic and transport properties of perovskite manganites.[55,56] In the following section, we will show that this effect has a considerable impact on the thermal and chemical expansion properties of $Dy_{1-x}Y_xMnO_{3+\delta}$.

3.3. Thermal and Chemical Expansion. Expansion of the crystal lattice can occur through two mechanisms: thermal expansion (TE) and chemical expansion (CE). TE, as discussed in tolerance factor arguments, is caused by expansion of the R−O and Mn−O bond lengths due to increased thermal energy at elevated temperature. CE is caused by expansion of the lattice due to changes in oxygen stoichiometry. Our TGA measurements of $Dy_{1-x}Y_xMnO_{3+\delta}$ materials, discussed at length in the previous section, have shown large changes in oxygen stoichiometry between two stable oxygen content regions, which occur upon heating over a relatively short time scale (≤2 h) and narrow range of temperatures (~100 °C). These characteristics allowed us to measure the effective CE over a narrow range of temperatures by simply subtracting the relatively small value of TE from the observed value of CE. Similarly precise measurements of TE, without any effect from CE, were possible in temperature regions of stable oxygen content. It should also be noted that, in some cases, the thermal expansion coefficient (TEC) is considered to be the net result of both CE and TE; here, we consider these to be separate effects, thus TEC in this report is only attributed to TE. The following equations were used to calculate TEC and CE:

$$\mathrm{TEC} = \frac{1}{L_0}\left(\frac{1}{n-m}\right)\sum_{i=m}^{n}\left(\frac{\Delta L_{i+1} - \Delta L_i}{T_{i+1} - T_i}\right)$$

measured in units of K^{-1}, where L_0, ΔL, and T are the sample starting length, the change in length, and the temperature, respectively, and m and n are the sets from the measured temperature ranges and

$$\mathrm{CE} = \frac{1}{\Delta\delta}\left[\left(\frac{\Delta L}{L_0}\right) - \langle \mathrm{TEC}\rangle \Delta T\right]$$

measured in units of $(\text{moles of O})^{-1}$, where $\Delta\delta$ is the absolute change in oxygen content from the stoichiometric value of 3.0

dx.doi.org/10.1021/cm2006956 |Chem. Mater. 2011, 23, 3818–3827

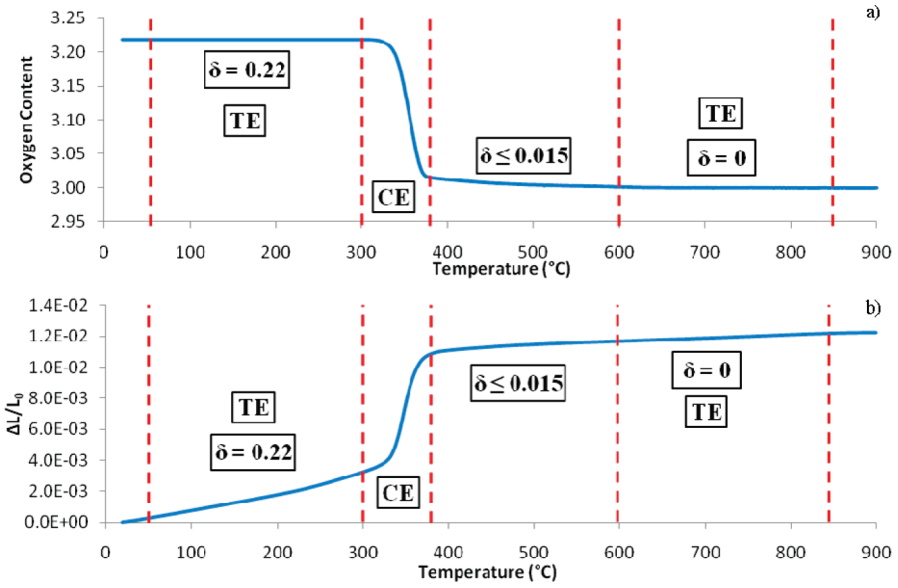

Figure 9. (a) TGA and (b) dilatometry measurements for $DyMnO_{3+\delta}$ in 21% O_2.

and ⟨TEC⟩ is the average TEC of the two oxygen-content-stable regions.

Pellets for dilatometry measurements were cut from dense samples (x = 0, 0.3, 0.5, 0.7, 1) after synthesis of the hexagonal material and were then annealed at 400 °C with cooling at a rate of 0.1 °C/min in O_2. The oxygen contents of these dense samples were also measured with identical conditions on TGA to determine the appropriate temperature ranges to separately extract TE and CE coefficients (the structural phases present and after dilatometry measurements were also confirmed with XRD). TE values were measured for these samples in their respective temperature regions of stable oxygen content observed in TGA for δ = 0.22−0.29 (∼50−300 °C) and for δ = 0 (∼600−850 °C). CE values were measured during the reduction between these stable oxygen contents over an approximate temperature gradient of ∼100 °C in the range of 240−390 °C, where ∼90% of the total oxygen reduction occurs. Figure 9 shows these measurements for $DyMnO_3$ and illustrates how the combination of dilatometry and TGA measurements was used to determine TE and CE for all $Dy_{1-x}Y_xMnO_{3+\delta}$ samples. The lower starting oxygen contents after annealing in oxygen and the slower reduction of dense pellets (as seen for $DyMnO_{3+\delta}$ in Figure 9a) versus the small chucks of material observed in Figure 4 during TGA measurement are due to the differences in the samples' density, surface area, and diffusion distances. The TEC values of the hexagonal phases in these two temperature regions of stable oxygen content were found to be quite different: $(8.2-10.2) \times 10^{-6}$ K^{-1} (δ = 0.22−0.29) and $(2.1-5.6) \times 10^{-6}$ K^{-1} (δ = 0), which indicates that the TEC values of the stoichiometric Hex_2 (δ = 0.25) and $P6_3cm$ phase are ∼$(8.4-11.6) \times 10^{-6}$ K^{-1} and $(2.1-5.6) \times 10^{-6}$ K^{-1}, respectively (Figure 10a). The CE values during a loss of oxygen content are $(0.82-3.48) \times 10^{-2}$ mol^{-1} (see Figure 10b), which increase significantly with Dy content.

Previous reports of single-crystal hexagonal $RMnO_3$ materials (R = Y, Ho, Sc, and Lu) have been shown to have lattice parameters that linearly increase in-plane and decrease along c with increasing temperature.[46,57] The contraction of the c-axis has also been shown to increase for larger R ions. Thus, the effect of substantial contraction of the c-axis is responsible for the observed

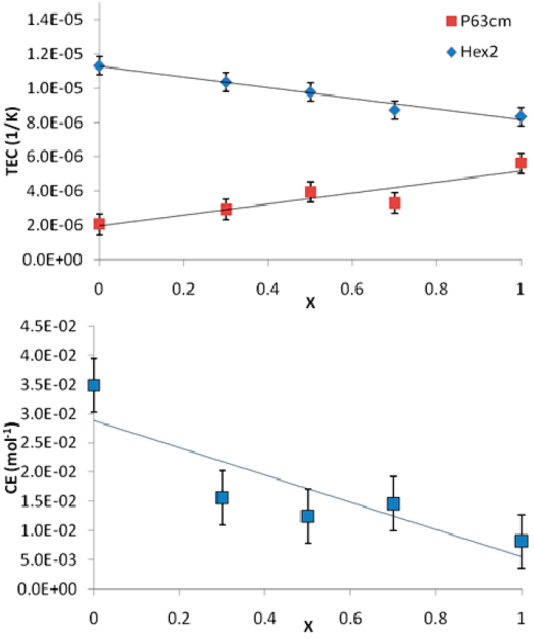

Figure 10. (a) TEC values for the $P6_3cm$ and Hex_2 phases and (b) chemical expansion (CE) parameter during the Hex_2-P6_3cm phase transition for $Dy_{1-x}Y_xMnO_{3+\delta}$.

small change of volume of the unit cell and significantly reduces the TE value of our polycrystalline $P6_3cm$ material, when compared to their Hex_2 or perovskite phases (7.3×10^{-6} K^{-1} and 6×10^{-6} K^{-1} for the perovskite phase of $DyMnO_3$ and $YMnO_3$, respectively[58,59]). It is also in agreement with the decrease in the net TE value with increased Dy content for $P6_3cm$ materials, as seen in Figure 10a. However, this tendency is reversed for the Hex_2 phase, which has been shown to have increased TEC values with increased Dy content. Finally, an increased rate of contraction along the c-axis at the Curie temperature, ∼650 °C, was reported previously for $YMnO_3$ and $HoMnO_3$ in one study,[57] but was also not observed in another report.[46] We did not observe any anomalous

dx.doi.org/10.1021/cm2006956 |Chem. Mater. 2011, 23, 3818–3827

behavior near this temperature; however, this effect may be beyond the sensitivity range of our dilatometer for a polycrystalline sample, where anisotropic effects are averaged out. On the other hand, if dense hexagonal $RMnO_3$ materials are also prone to small nonstoichiometric behavior upon heating, as seen here for the temperature range of 400−600 °C ($0 < \delta < 0.015$), this effect could be due to the CE associated with the reduction of a slightly oxygenated sample to stoichiometric oxygen content. Our measurements show the importance of understanding oxygen content behavior, as slight changes in oxygen content can have similar effects on the net expansion as structural changes, which are not associated with changes in oxygen content (e.g., the $P6_3cm$ to $P6_3/mmc$ phase transition).

The CE value during the transition from the mixed-state $Hex_2/P6_3cm$ (~85%−100%, $\delta \approx 0.22-0.25$) materials, relative to that of almost single-phase $P6_3cm$ has a much larger effect on the total expansion than the TE value. As discussed with the tolerance factor arguments, the primary cause of the CE seen during the $P6_3cm/Hex_2$ transition is due to the change in ionic radius of the $Mn^{(3+2\delta)+}$ cation. Finally, for comparison, the CE values reported here are of the same order of magnitude as the CE associated with the absorption and desorption of oxygen in perovskite $LaMnO_3$ or similar substituted perovskite manganites (~2.4×10^{-2} mol^{-1} and ~$(1-4) \times 10^{-2}$ mol^{-1}).[60−62] However, the effect of CE for the hexagonal structure is much more prominent than in the perovskite phase, because of the larger change in oxygen content, occurring over a much narrower temperature range.

4. CONCLUSIONS

Our synthesis results and previous work with perovskite manganites suggest that increasingly stronger reducing conditions are needed to form hexagonal $Dy_{1-x}Y_xMnO_{3+\delta}$ with decreasing x (for $x \leq 0.7$). Previous reports of synthesis of the perovskite phase from the hexagonal phase with smaller rare earths (Ho, Er, and Y), under high pressure, support the argument that transformations occur at specific values of the tolerance factor, because of the temperature, oxygen nonstoichiometry, and compressibility dependence of the R−O and Mn−O bond lengths. Hexagonal $Dy_{1-x}Y_xMnO_{3+\delta}$ materials were observed to reversibly absorb large amounts of oxygen at ~200 − 300 °C and to sharply desorb oxygen during transition back to the stoichiometric $P6_3cm$ phase above ~275−375 °C or at lower temperatures in lower partial pressures of oxygen. Increased reversible changes in oxygen content were achieved by annealing at high pressures ($\delta = 0.25-0.35$) and with hydrogen reduction at 400 °C (δ values between −0.12 and −0.20), which, if combined, can yield reversible oxygen storage capacities (OSCs), up to ~2650 μmol-O/g. Rates of oxygen absorption were also observed to decrease significantly with increasing yttrium content. The thermal expansion (TE) values of the Hex_2 and $P6_3cm$ phases were determined to be quite different: $(8.4-11.6) \times 10^{-6}$ K^{-1} and $(2.1-5.6) \times 10^{-6}$ K^{-1}, respectively, and the chemical expansion associated with the transition between these phases was found to be $(0.82-3.48) \times 10^{-2}$ mol^{-1}. The nonstoichiometric oxygen content of these hexagonal manganites no doubt has profound influence on their multiferroic properties. We are currently measuring these new structural phases of the $Dy_{1-x}Y_xMnO_{3+\delta}$ system with neutron powder diffraction, as well as studying their magnetic and transport properties.

AUTHOR INFORMATION

Corresponding Author

*Phone: 217-377-8884. Fax: 815-753-8565. E-mail: sremsen@gmail.com.

ACKNOWLEDGMENT

We thank Dr. David Carter (Chemical Sciences and Engineering Division of Argonne National Laboratory) for fruitful discussions and James Mais, Stephen Boona, and Donald Johnson for their laboratory support at Northern Illinois University. This work was supported by the Division of Materials Sciences and Engineering Division of the Office of Basic Energy Sciences, U.S. Department of Energy Office of Science, under Contract No. DE-AC02-06CH11357.

REFERENCES

(1) Shelley, S. *Chem. Eng. Prog.* **2009**, *105*, 6.
(2) Kašpar, J.; Fornasiero, P.; Hickey, N. *Catal. Today* **2003**, *77*, 419.
(3) Kodama, T.; Gokon, N. *Chem. Rev.* **2007**, *107*, 4048.
(4) Xu, Z.; Qi, Z.; Kaufman, A. *Power Sources* **2003**, *115*, 40.
(5) Sakakini, B.; Taufig-Yap, Y.; Waugh, K. *J. Catal.* **2000**, *189*, 253.
(6) Ciferno, J.; et al. Technical Paper DOE/NETL-2007/1291, 2007.
(7) Rydén, M.; Lyngfelt, A.; Mattisson, T.; Chen, D.; Holmen, A.; Bjørgum, E. *Int. J. Greenhouse Gas Control* **2008**, *2*, 21.
(8) Klara, J.; et al. Technical Paper DOE/NETL-2008/1307, 2007.
(9) Readman, J.; Olafsen, A.; Larring, Y.; Blom, R. *Mater. Chem.* **2005**, *15*, 1937.
(10) Figueroa, J.; Fout, T.; Plasynski, S.; McIlvried, H.; Srivastava, R. *Int. J. Greenhouse Gas Control* **2008**, *2*, 9.
(11) Pei, S.; Kleefisch, M.; Kobylinski, T.; Faber, J.; Udovich, C.; Zhang-McCoy, V.; Dabrowski, B.; Balachandran, U.; Mieville, R.; Poeppel, R. *Catal. Lett.* **1995**, *30*, 201.
(12) He, H.; Dai, H. X.; Au, C. T. *Catal. Today* **2004**, *90*, 245.
(13) DiMonte, R.; Fornasiero, P.; Graziani, M.; Kašpar, J. *J. Alloys Compd.* **1998**, *275*, 887.
(14) Nagai, Y; Yamamoto, T.; Tanaka, T.; Yoshida, S.; Nonaka, T.; Okamoto, T.; Suda, A.; Sugiura, M. *Catal. Today* **2002**, *74*, 225.
(15) Singh, P.; Hegde, M.; Gopalakrishnan, J. *Chem. Mater.* **2008**, *20*, 7268.
(16) Karppinen, M.; Yamauchi, H.; Otani, S.; Fujita, T.; Motohashi, T.; Huang, Y.; Valkeapää, M.; Fjellvag, H. *Chem. Mater.* **2006**, *18*, 490.
(17) Motohashi, T.; Kadota, S.; Fjellvag, H.; Karppinen, M.; Yamauchi, H. *Mater. Sci. Eng., B* **2008**, *148*, 196.
(18) Kadota, S.; Karppinen, M.; Motohashi, T.; Yamauchi, H. *Chem. Mater.* **2008**, *20*, 6378.
(19) Räsänen, S.; Motohashi, T.; Yamauchi, H; Karppinen, M. *J. Solid State Chem.* **2010**, *183*, 692.
(20) Chmaissem, O.; Zhen, H.; Huq, A.; Stephens, P.; Mitchell, J. *J. Solid State Chem.* **2008**, *181*, 664.
(21) Rydén, M.; Lyngfelt, A.; Mattisson, T.; Chen, D.; Holmen, A.; Bjørgum, E. *Int. J. Greenhouse Gas Control* **2008**, *2*, 21.
(22) Readman, J.; Olafsen, A.; Larring, Y.; Blom, R. *J. Mater. Chem.* **2005**, *15*, 1937.
(23) Motohashi, T.; Ueda, T.; Masubuchi, Y.; Takiguchi, M.; Setoyama, T.; Oshima, K.; Kikkawa, S. *Chem. Mater.* **2010**, *22*, 3192.
(24) Yakel, H. L.; Koehler, W. C.; Bertaut, E. F.; Forrat, E. F. *Acta Crystallogr.* **1963**, *16*, 957.
(25) Yakel, H. L. *Acta Crystallogr.* **1955**, *8*, 394.
(26) Shannon, R. D. *Acta. Crystallogr., Sect. A: Cryst. Phys., Diffr., Theor., Gen. Crystallogr.* **1976**, *32*, 751.
(27) Dabrowski, B.; Chmaissem, O.; Mais, J.; Kolesnik, S.; Jorgensen, J. D.; Short, S. *J. Solid State Chem.* **2003**, *170*, 154.

(28) Dabrowski, B.; Remsen S. U.S Patent Application No. 61/407,580, filing date Oct. 28, 2010.
(29) Dabrowski, B.; Kolesnik, S.; Baszczuk, A.; Chmaissem, O.; Maxwell, T; Mais, J. *J. Solid State Chem.* **2005**, *178*, 629.
(30) Kamegashira, N.; Satoh, H.; Ashizuka, S. *Mater. Sci. Forum* **2004**, *449*, 1045.
(31) Park, J.; Park, J. G.; Jeon, G. S.; Choi, H. Y.; Lee, C.; Jo, W.; Bewley, R.; McEwen, K. A.; Perring, T. G. *Phys. Rev. B* **2003**, *68*, 104426.
(32) Lee, S.; Pirogov, A.; Han, J. H.; Park, J. G.; Hoshikawa, A.; Kamiyama, T. *Phys. Rev. B* **2005**, *71*, 180413(R).
(33) Ivanov, V. Y.; Mukhin, A. A.; Prokhorov, A. S.; Balbashov, A. M.; Iskhakova, L. D. *Phys. Solid State* **2006**, *48*, 1726.
(34) Carp, O.; Patron, L.; Ianculescu, A.; Pasuk, J.; Olar, R. *J. Alloys Compd.* **2003**, *351*, 314.
(35) Szabo, G.; Paris, R. A. *C. R. Seances Acad. Sci., Ser. C* **1969**, *268*, 517.
(36) Brinks, H. W.; Fjellvág, H.; Kjekshus, A. *J. Solid State Chem.* **1997**, *129*, 334.
(37) Suescun, L.; Dabrowski, B.; Mais, J.; Remsen, S.; Richardson, J. W., Jr.; Maxey, E. R.; Jorgensen, J. D. *Chem. Mater.* **2008**, *4*, 1636.
(38) Zhou, J. S.; Goodenough, J. B.; Gallardo-Amores, J. M.; Morán, E.; Alario-Franco, M. A.; Caudillo, R. *Phys. Rev. B* **2006**, *74*, 014422.
(39) Waintal, A.; Chenavas, J. *Mater. Res. Bull.* **1967**, *2*, 819.
(40) Tachibana, M.; Shimoyama, T.; Kawaji, H.; Atake, T.; Takayama-Muromachi, E. *Phys. Rev. B* **2007**, *75*, 144425.
(41) Uusi-Esko, K.; Malm, J.; Imamura, N.; Yanauchi, H.; Karppinen, M. *Mater. Chem. Phys.* **2008**, *112*, 1029.
(42) Remsen, S.; Dabrowski, B. Unpublished data.
(43) Lonkai, Th.; Tomuta, D. G.; Amann, U.; Ihringer, J.; Hendrikx, R. W. A.; Többens, D. M.; Mydosh, J. A. *Phys. Rev. B* **2004**, *69*, 134108.
(44) Jeong, I.; Hur, N.; Proffen, T. *J. Appl. Crystallogr.* **2007**, *40*, 730.
(45) Kamata, K.; Nakajima, T.; Nakamura, T. *Mater. Res. Bull.* **1979**, *14*, 1007.
(46) Katsufuji, T.; Masaki, M.; Machida, A.; Moritomo, M.; Kato, K.; Nishibori, E.; Takata, M.; Sakata, M.; Ohoyama, K.; Kitazawa, K.; Takagi, H. *Phys. Rev. B* **2002**, *66*, 134434.
(47) Zhou, J. S.; Goodenough, J. B.; Gallardo-Amores, J. M.; Morán, E.; Alario-Franco, M. A.; Caudillo, R. *Phys. Rev. B* **2006**, *74*, 014422.
(48) Fiebig, M.; Lottermoser, T.; Pisarev, R. V. *Appl. Phys.* **2003**, *93*, 8194.
(49) Vajik, O. P.; Kenzelmann, M.; Lynn, J. W.; Kim, S. B.; Cheong, S. W. *Phys. Rev. Lett.* **2005**, *94*, 087601.
(50) Lonkai, Th.; Tomuta, D. G.; Amann, U.; Ihringer, J.; Hendrikx, R. W. A.; Többens, D. M.; Mydosh, J. A. *Phys. Rev. B* **2004**, *69*, 134108.
(51) Jeong, I.; Hur, N.; Proffen, T. *Appl. Crystallogr.* **2007**, *40*, 730.
(52) Rao, C. N. R.; Serrao, C. R. *Mater. Chem.* **2007**, *17*, 4931.
(53) Choi, W. S.; Kim, D. G.; Seo, S. S. A.; Moon, S. J.; Lee, D.; Lee, J. H.; Lee, H. S.; Cho, D. Y.; Lee, Y. S.; Murugavel, P.; Yu, J.; Noh, T. W. *Phys. Rev. B* **2008**, *77*, 045137.
(54) Nandi, S.; Kreyssig, A.; Yan, J.; Vannette, M.; Lang, J.; Tan, L.; Kim, J.; Prozorov, R.; Lograsso, T.; McQueeny, R.; Goldman, A. *Phys. Rev. B* **2008**, *78*, 075118.
(55) Dabrowski, B.; Klamut, P. W.; Bukowski, Z.; Dybzinski, R.; Siewenie, J. E. *J. Solid State Chem.* **1999**, *144*, 461.
(56) Bukowski, Z.; Dabrowski, B.; Mais, J.; Klamut, P. W.; Kolesnik, S.; Chmaissem, O. *J. Appl. Phys.* **2000**, *9*, 5031.
(57) Zhou, H. D.; Denyszyn, J. C.; Goodenough, J. B. *Phys. Rev. B* **2005**, *72*, 224401.
(58) Remsen, S. Ph.D. Dissertation, Northern Illinois University, DeKalb, IL, 2010.
(59) Fu, B.; Huebner, W. *Mater. Res.* **1994**, *9*, 2645.
(60) Chen, X.; Yu, J.; Adler, S. B. *Chem. Mater.* **2005**, *17*, 4537.
(61) Miyoshi, S.; Hong, J.; Yashiro, K.; Kaimai, A.; Nigara, Y.; Kawamura, K.; Kawada, T.; Mizusaki, J. *Solid State Ionics* **2003**, *161*, 209.
(62) McIntosh, S.; Vente, J. F.; Haije, W. G.; Blank, D.; Bouwmeester, H. *Chem. Mater.* **2006**, *18*, 2187.